

Estimation of additional PV Converter Losses operating under $PF \neq 1$ based on Manufacturer's Data at $PF=1$

Kyriaki-Nefeli D. Malamaki, and Charis S. Demoulias

Abstract—The increasing penetration of Photovoltaic (PV) systems in distribution networks often causes overvoltage problems. One solution to address this issue is the provision of reactive power (RP) by the PV converters. This can cause increased power losses on the PV converters leading to additional operational costs. However, the manufacturers of commercially available PV converters provide data regarding the converter losses only under unity power factor (PF). The data are also limited regarding the technical details of the PV converters. This paper presents a methodology to estimate analytically the power losses in two-stage PV converters under RP provision based on the efficiency curves at $PF=1$ for different PV voltages and the limited information given in the PV converter datasheet. The losses are separately estimated for the DC/DC converter and the DC/AC inverter, because the losses on the former are not affected by the RP, while the losses on the latter are. The method is validated with field measurements of PV converter losses under RP provision and with detailed simulations.

Index Terms—Efficiency of PV Converters, Power Losses of PV Converters, Reactive power, Pulse width modulation converters, Photovoltaic systems, Power generation control.

I. INTRODUCTION

Photovoltaics (PV) are predicted to become the biggest contributor to electricity generation among all renewable energy candidates by 2040 [1]. However, the most common problem caused by the high PV penetration is the voltage rise due to reverse power flow, both at Medium-Voltage and Low-Voltage (LV) level [2]. Various solutions have been suggested to address it, but the most promising from technical and financial point of view has been shown to be the exchange of reactive power (RP) from the distributed PV systems [3-6], even at the LV level, where high R/X ratios prevail. For this reason, some grid codes (in Germany, Italy, Austria, UK, France [7, 8]) impose the RP capability of DRES as a mandatory system support function in order to allow their grid connection. More specifically, it is required that the DRES exchange RP either according to local measurements of the voltage and injected power [9] or according to signals sent by the Distribution Network Operators [10]. These solutions address the voltage regulation in a sufficient way. Nevertheless, they mostly ignore the PV converter (PVC) operational cost due

to the RP exchange. As RP is mostly needed under high active power injection, the new PVCs need to be oversized in order to avoid active power curtailment [11], leading to increased purchase cost and efficiency reduction [12].

The future Smart Grids will use the PVC RP capability for voltage regulation purposes as a new ancillary service (AS) provided at distribution system level [13]. Currently only the RP provided by conventional synchronous generators at transmission level is considered as AS and is traded in the respective AS market. It is noted that the additional losses incurred in their excitation system and stator are taken into account as operational cost for the proper RP remuneration in those AS markets [14]. Therefore, the additional purchase (due to oversizing) and operational (due to power and energy losses) costs for the PVCs must be quantified in order to be able to be remunerated, as well.

Nowadays, the PVC manufacturers provide efficiency curves only at power factor (PF)=1 as function of the PVC output power, for 2 or 3 input DC voltages, – as in Fig. 1 [15, 24]. They also do not provide information about technical details for the power switches, filters, PWM switching frequency, etc. They do mention the number of Maximum Power Point Tracking (MPPT) inputs, i.e. the number of DC/DC converters, and the PF limits within which the PVC can operate [15,16].

Although there are many mathematical models describing the PVC efficiency curve [12,17,18] in association with the DC voltage and power level, all of them refer to $PF=1$. The losses incurred to the PVC at $PF \neq 1$ have been so far addressed to a very limited extent, [19-23]. In [19] the operation of a specific three-phase (3ph) inverter has been tested at Sandia National Laboratories and then modelled in MATLAB/Simulink at $PF \neq 1$. The results showed that RP provision leads to PVC efficiency decrease. In [20] four Volt/Var control methods are tested in a specific 3ph inverter in the same laboratory. The effects of these methods on the inverter efficiency, the real power delivered to the grid and on the inverter service life are discussed for each control method. An empirical expression is derived associating the losses to the PF , output current and PV voltage. However, this expression was determined through trial

This work is part of the EASY-RES project that has received funding from the European Union's Horizon 2020 Research and Innovation programme under Grant Agreement No 764090.

K.-N. D. Malamaki (e-mail: kyriaki_nefeli@hotmail.com) and C. S. Demoulias (e-mail: chdimoul@auth.gr) are with the Department of Electrical and Computer Engineering, Aristotle University of Thessaloniki, Thessaloniki 54124, Greece.

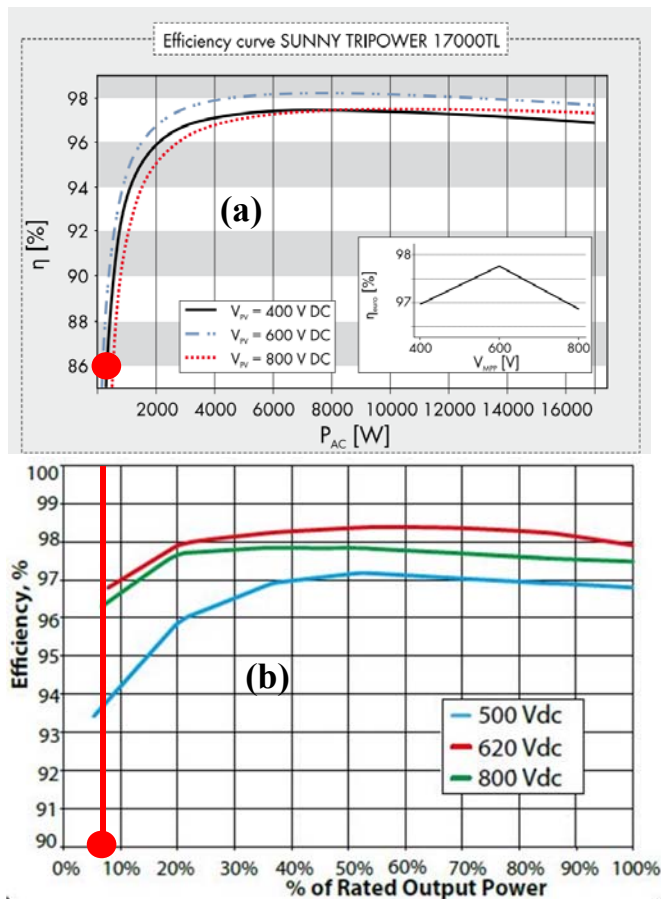


Fig. 1. Efficiency Curves at 3 different input voltages (V_d) for a PVC (a) of SMA 17kVA [15]; (b) of ABB 20kVA [24]

and error and is not expected to be unique, because it concerns a specific 25kVA PVC.

In [21] the switching and conduction losses of IGBTs and diodes are analytically expressed for two different inverter topologies (single-phase, two-level, H-bridge and three-level NPC half-bridge inverter) based on the knowledge of the switches' details (forward voltages, junction-to-case thermal resistance, etc.). Their results are compared to simulation of such converters with detailed IGBT and diode models in Simulink environment. The modulation index m was taken in all cases equal to 1. In [22, 23] single-phase (1ph) PV H-bridge inverters are simulated in MATLAB/Simulink and PowerSim, respectively, under the operation at non-unity PFs. The results of the simulation and impacts of RP provision on the diodes and IGBTs conduction power losses (switching losses are ignored), thermal behavior (temperature rise) and deterioration in life expectancy of the switches are discussed. In [22] a reliability analysis is performed based on a yearly thermal loading profile of the PV inverter together with a cost-benefit analysis of RP provision to the grid outside the feed-in hours. In [23] it is proved through simulations that the losses and temperature rise are slightly higher at leading PFs compared to the lagging PF for the same PF value due to the fact that the inverter output voltage is higher for lagging PF operation. In all of these studies, only the inverter losses are examined, since they are affected electrically and thermally by $PF \neq 1$. However, most

commercially available converters have at least one MPPT input [15,16,24]. Furthermore, all the evaluations of the power losses in [19-23] (either analytically or by simulation) depend on the knowledge of the aforementioned technical details of the PVC elements (switches, etc). However, such details are not provided in the manufacturer's datasheets and it is quite difficult to simulate a commercially available PVC without knowing the technical details. Therefore, there is no generic method for estimating the power losses of the PVCs operating at $PF \neq 1$ from the rough data provided in the datasheets, especially with the existence of a DC/DC converter, when the DC-link voltage V_{DC-L} is not given.

To fill this gap, this paper presents an analytical tool for estimating the power losses on PVCs under $PF \neq 1$ based on the limited information given in the manufacturers' datasheet for $PF=1$. The power losses are separated in the conduction, switching and filter losses on the boost converters and on the inverter. The latter depend on the PF, while the former do not.

The novelty of this methodology lies to the separation of the losses on the boost converter and inverter, when given are only the aggregated losses for $PF=1$ and the operating points of the whole PVC. For this reason, the DC/DC converter losses are expressed as function of the PV string parameters, i.e. PV voltage and power, while the inverter losses are expressed as function of the AC output voltage, power and PF. Also, the shape of the efficiency curves for various PV voltages is exploited together with basic power electronics theory [25] to evaluate whether the DC/DC converter operates at continuous (CCM) or discontinuous conduction mode (DCM).

The validity of the proposed tool was tested with field measurements of the losses of existing PVCs operating at various PFs in the range of 0.8 leading to 0.8 lagging with the respective DC/DC converters operating at DCM. In addition to field measurements, detailed simulations were conducted to test the validity of the tool when the DC/DC converter operates at CCM while the inverter operates as current-controlled voltage source.

The proposed tool is suitable for the commonly used 1ph or 3ph string PVCs, which consist of: a H-4 or H-6 bridge inverter and one or more non-isolated type DC/DC boost converters utilized for performing the MPPT tasks. It is also suitable for the rare cases, where the PVC consists only of an H-bridge inverter.

II. THEORETICAL FRAMEWORK AND POWER LOSSES MATHEMATICAL MODELS

In most PVC datasheets the efficiency curves are given at $PF=1$ for 2 or 3 different PV voltage levels (V_d), as shown in Fig.1. In some cases, the manufacturer provides a general outline of the PVC topology [16,24], e.g. whether it contains a transformer, where capacitors and filters are placed, etc. In cases such an outline does not exist, one can guess the existence and the number of DC/DC converters from the number of DC inputs with MPPT capability, each of which can operate at different V_d . Several other details concerning the DC/DC converter, the inverter (full-bridge, half-bridge, H-6 or H-5), filter magnitude, switching frequency, PVC control method,

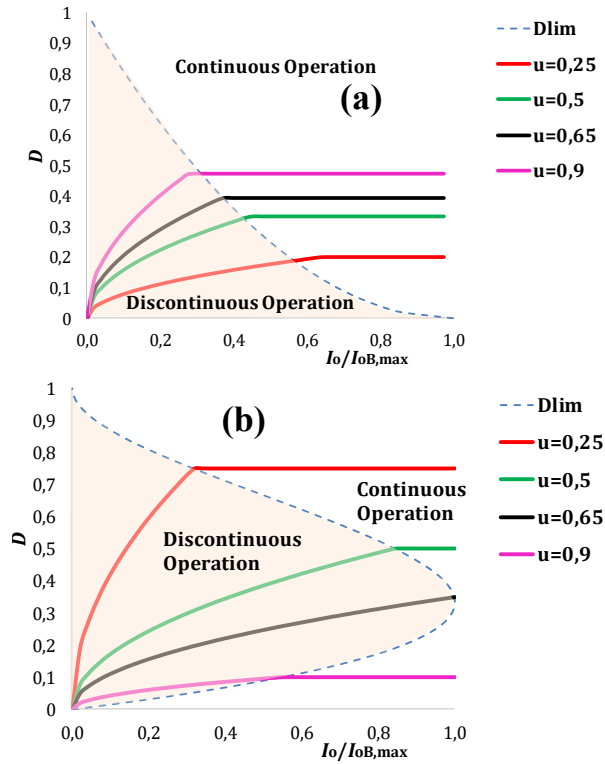


Fig.2. Graphs showing the boundary between CCM and DCM for (a) buck-boost and (b) boost DC/DC converters with $u=V_d/V_{DC-L}$ as parameter.

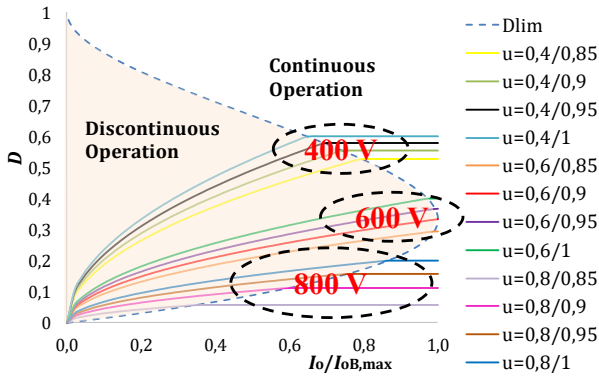


Fig.3 The Duty cycle D as function of the ratio $I_o/I_{oB,max}$ for three different input voltages V_d and ratio $u=V_d/V_{DC-L}$ as parameter for the converter of [15].

etc., are omitted in the PVC datasheet.

In case the PVC datasheet mentions that the PVC has MPPT capability over a wide range of PV voltages, then, apart from the inverter, there is a DC/DC converter. Currently the most preferred DC/DC converters are the buck-boost and the boost converter due to their simplicity [26], [38]. However, usually, there is no information about the type of the DC/DC converters, i.e. whether they are boost or buck-boost. This information can be derived by observing the number of efficiency curves (Fig.1), where one efficiency curve per V_d is given. While some manufacturers provide the type of the DC/DC converter [16], others omit this information (Fig.1(b)-[24]). Nevertheless, the common thing in both cases of Fig. 1 is that the highest efficiency (hence, lowest losses) appears in the “median” V_d . This can be explained considering the following analysis which

is based on the operating principles of basic non-isolated DC/DC topologies:

In PV applications the inverter maintains V_{DC-L} constant, while the DC/DC converter performs MPPT (Fig. A1 in the Appendix). For given V_{DC-L} the power losses on the DC/DC converter depend on V_d and on the PV power, P_{in} . The value of V_d is determined by the duty cycle D of the DC/DC converter switch. Moreover, according to the overall design of the DC/DC converter, it may operate at DCM or CCM depending on its loading, i.e., the output current I_o . This dependence can be derived analytically for the two types of DC/DC converters by using the following expressions per converter type [25]:

Boost :

$$I_{oB,max} = \frac{2V_{DC-L}}{27Lf_{sw}} \quad (a) \quad (1)$$

$$CCM : D = 1 - \frac{V_d}{V_{DC-L}} \quad (b)$$

$$DCM : D = \frac{2}{3V_d} \sqrt{3I_o V_{DC-L} (V_{DC-L} - V_d)} \quad (c)$$

$$I_{oB} = \frac{27}{4} I_{oB,max} D(1-D)^2 \quad (d)$$

Buck – Boost :

$$I_{oB,max} = \frac{V_{DC-L}}{2Lf_{sw}} \quad (a) \quad (2)$$

$$CCM : D = \frac{V_{DC-L}}{V_{DC-L} + V_d} \quad (b)$$

$$DCM : D = \frac{V_{DC-L}}{V_d} \sqrt{\frac{I_o}{I_{oB,max}}} \quad (c)$$

$$I_{oB} = I_{oB,max} (1-D)^2 \quad (d)$$

Using the above equations, graphs (Fig. 2) showing whether the DC/DC converter operates in DCM or CCM can be drawn as a function of the duty cycle D and the converter loading expressed via the ratio $I_o/I_{oB,max}$, where $I_{oB,max}$ is the maximum value of the boundary output current I_{oB} . As can be noticed in Fig. 2(a), increasing V_d , for the same loading, moves the buck-boost converter closer to the DCM. Further increase of V_d will keep this converter type within the DCM region. The latter is explained by the fact that (2d) is a second order function, i.e., it is monotonous. On the contrary, (1d) is a third order function, i.e., it is not monotonous, as shown in Fig.2(b) for the boost converter. With given loading of this converter type, it may operate at CCM with low V_d , then enter the DCM as V_d increases and finally, operate again in CCM as V_d increases further. Therefore, the boost converter may operate at DCM for “median” values of V_d , while for larger or lower values of V_d it may operate at CCM. Since the DCM operation means lower losses and higher efficiency, it is expected that in a boost converter the highest efficiency will appear in this “median” voltage within the range of V_d that is allowed by the PVC datasheet. Therefore, when observing a figure similar to Fig. 1, where the efficiency at 600V (Fig. 1(a)) or at 620V (Fig. 1(b)), is higher than at 400, 500 or 800V, it can be concluded that the DC/DC converter involved is a boost one.

A graph like Fig. 2(b) can be derived provided that V_d and

V_{DC-L} are known. However, the PVC datasheets contain information only about V_d [15,24], while the value of V_{DC-L} is omitted. The range of V_{DC-L} can be estimated after reasonable engineering assumptions: in case there is a boost converter, obviously, the minimum V_{DC-L} is higher than the highest V_d . In case of a buck-boost converter the minimum V_{DC-L} can be assumed to be 700V, since below this value the inverter would operate in the over-modulation region when connected to a 400V, 50Hz grid, leading to increased harmonic distortion of the injected currents [36]. The maximum value of V_{DC-L} can be considered as 1kV for the following reasons: the duty cycle, D , of boost and buck-boost converters is limited to below 0.6, in order to maintain high efficiency and controllability [25]. This value of D together with the lower V_d for CCM determines the maximum value of V_{DC-L} together with the fact the 1kV is close to the upper limit for an equipment to conform for LV installations. As an example, for the PVC of Fig.1(a), $V_{d,min}=400V$ and $D=0.6$ yields $V_{DC-L}=1kV$.

Based on the aforementioned analysis, Fig. 3 has been drawn using (1) and it depicts the required D as function of $I_o/I_{oB,max}$ for the three different V_d , 400V, 600V and 800V given by the manufacturer with V_{DC-L} ranging from 850V to 1kV. The curve D_{lim} shows the ratios $I_{oB}/I_{oB,max}$, i.e. the Boundary Condition. As it can be observed in Fig. 3, the boost converter operates at DCM for the whole power range when $V_d=600V$ for any V_{DC-L} within the possible range of 850V-1kV.

It is now evident from the above analysis, the reason why most PVC manufacturers prefer boost instead of buck-boost converters: for a given range of V_d and V_{DC-L} , it is much easier for a boost converter to operate at DCM, i.e., at higher efficiency, for almost the full range of power, while a buck-boost would operate at DCM only at very low loading conditions (compare Fig. 2(a) with Fig. 2(b)). Additionally, in [26] it is mentioned that the two-stage PVC consisting of (i) a boost converter for MPPT and (ii) an inverter with high-frequency PWM control method, is a commonly used PVC topology.

The above analysis is essential for the determination of the DC/DC converter type, since already known expressions will be used in order to derive the method presented in this paper. As shown in the Appendix, the total inverter losses can be expressed as a function of the output power P_o , the converter rated power S_b , the filter reactance $x_{f(pu)}$ expressed in per unit and the operating $PF=\cos\varphi$

$$P_{loss}^{Inv} = c_1 + c_2 \frac{P_o}{PF} + c_3 \frac{P_o^2}{PF^2} + P_o \left(c_4 + c_5 \frac{P_o}{PF} \right) \cdot \sqrt{\left(\frac{x_{f(pu)} \cdot P_o}{S_b} \right)^2 + \left(\frac{x_{f(pu)} \cdot P_o}{S_b} \tan \varphi + 1 \right)^2} \quad (3)$$

while the DC/DC converter losses can be expressed as a function of converter input power P_{in}

$$P_{loss-CCM}^{Boost} = P_{in} \cdot (c_6 + c_7 P_{in}) \quad (4a)$$

$$P_{loss-DCM}^{Boost} = P_{in} \cdot (c'_6 + c'_7 P_{in}) + \sqrt{P_{in}} (c'_8 + c'_9 P_{in}) \quad (4b)$$

Therefore, the total PVC losses, P_{total}^{PVC} , can be expressed as either $P_{total-CCM}^{PVC}$ or $P_{total-DCM}^{PVC}$ under CCM or DCM

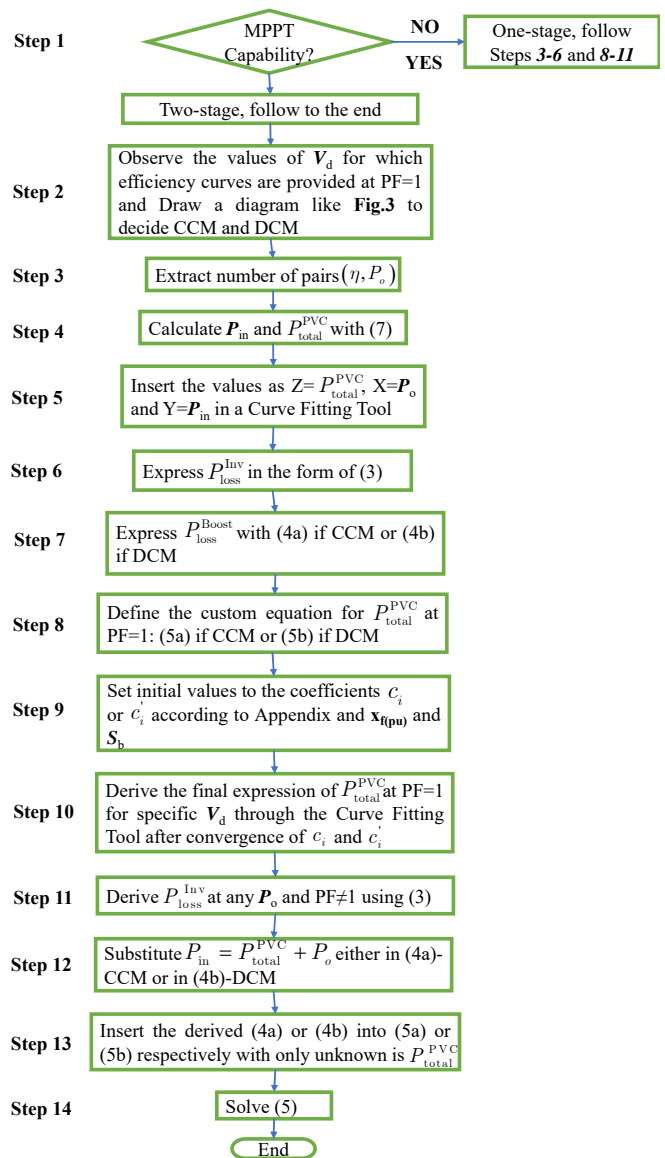


Fig. 4 Flow-Chart of the Proposed Methodology

respectively,

$$P_{total-CCM}^{PVC} = P_{loss}^{Inv}(P_o, PF) + P_{loss-CCM}^{Boost}(P_{in}) \quad (5a)$$

$$P_{total-DCM}^{PVC} = P_{loss}^{Inv}(P_o, PF) + P_{loss-DCM}^{Boost}(P_{in}) \quad (5b)$$

It can be noticed that (4) does not include the PF. This is reasonable since the DC/DC converter cannot regulate any RP. This can be done only by the inverter through the control of the amplitude and phase of the injected AC currents. For this reason, the PF appears only in (3). The losses on both converters depend on the voltages and currents as analytically derived in Appendix. Therefore, they can be expressed as functions of P_{in} and P_o . This was done because usually the losses and the efficiency are demonstrated as function of the PVC loading in terms of power and because the power is something easy to measure.

The coefficients c_i and c'_i in (3) and (4) are actually functions of:

(i) converter hardware parameters (as shown in the Appendix)

that are unknown as they are normally not provided by the manufacturer. These parameters are properties of a given PVC hardware and are affected by their temperature. However, the cooling system of the PVC maintains the internal temperatures within the permissible levels. Thus, it can be said that these hardware parameters are only slightly affected by the PVC ambient and loading conditions, as the internal junction temperature is kept more or less constant through the surveillance of the cooling system. It is noted that under extreme ambient conditions the PVC enters a power-derating mode taking a feedback from its cooling system. However, the losses in such abnormal operating conditions are not examined in this paper.

(ii) other operating parameters, such as the PV string voltage, V_d and the AC grid voltage V_g .

It is also noted that the coefficients c_i and c'_i in (3) and (4) are not functions of the PF (see Appendix). It is important to note that (3) was derived in such a way so as to “isolate” the PF outside any other coefficient. The coefficients c_i and c'_i in (3) and (4) can be determined following the methodology proposed below, if a sufficient dataset is given. This dataset is the efficiency curve as function of the PVC loading that is normally provided by the PVC manufacturer for PF=1 under various PV string voltages, V_d , and for given AC grid voltage V_g . Determining these coefficients, subsequently allows the estimation of the converter losses at any PF using (3)-(5). As shown in Appendix, $c_i=c'_i=0$, for $i \geq 6$ in case a boost converter is absent.

III. PROPOSED METHODOLOGY

The proposed methodology is based on:

- the separation of the losses on the DC/DC converter and the inverter in case the PVC is a two-stage one
- estimating the coefficients c_i and c'_i in (3) and (4) by setting initial values for those coefficients using data provided by the PVC manufacturer for PF=1 and following reasonable technical constraints

A. Separation of the Losses at non-unity PF

Based on the theoretical framework presented in the previous section, and observing the PVC datasheet, the steps for deriving the P_{total}^{PVC} are the following:

(I) Check the PVC leaflet to see if the PVC has MPPT capability over a wide range of PV voltages: If “YES”, then the PVC is a two-stage one, if “NO”, it is one-stage. If the PVC is a two-stage one, then, follow steps (2) to the end, if not, follow steps (3)-(6) and (8)-(11).

(2) Observe the values of PV voltages V_d for which the efficiency curves are provided for PF=1. Using the aforementioned reasoning, the possible range of V_{DC-L} can be estimated. For example, $850V < V_{DC-L} < 1kV$ in case the efficiency curves are the ones in Fig.1(a) or Fig. 1(b). A diagram similar to Fig. 3 can be derived using (1) in order to decide for which V_d the converter operates at CCM or DCM.

(3) Extract a number of pairs (η, P_o) of efficiency, η vs PVC output power P_o , from the efficiency curve for a specific V_d and PF=1. The extraction can be made using any software (e.g. GetData Graph Digitizer [37]) that can extract points from a

diagram. An alternative way to obtain these pairs is to express mathematically the specific efficiency curve using the simple method mentioned in [12] as

$$\eta(P_{o,pu}) = A + B \cdot P_{o,pu} + \frac{C}{P_{o,pu}} \quad (6)$$

Parameters A , B and C can be easily calculated by: (i) choosing three pairs of $(\eta, P_{o,pu})$ that correspond to $P_{o,pu}=0.1, 0.2$ and 1 pu from the PVC efficiency curve; (ii) solving the system of the three linear equations with three unknowns. The number of pairs should be more than 50, so as the curve-fitting approach mentioned in the following steps is effective.

(4) Calculate P_{in} and P_{total}^{PVC} with:

$$P_{in} = \frac{P_o}{\eta} \quad (a)$$

$$P_{total}^{PVC} = P_o \cdot \left(\frac{1}{\eta} - 1 \right) \quad (b)$$

(5) insert the values derived in step (4) as $Z=P_{total}^{PVC}$, $X=P_o$ and $Y=P_{in}$ in a Curve Fitting Tool (e.g. the one in MATLAB)

(6) Express the P_{loss}^{inv} in the form of (3) using (A2), (A4) and (A14) in Appendix; they correspond to filter, conduction and switching losses.

(7) Express the losses on the DC/DC converter:

a) In case of a boost converter at CCM express $P_{loss-CCM}^{Boost}$ in the form of (4a) using (A1), (A9) and (A15) presented in the Appendix.

b) In case of a boost converter at DCM express $P_{loss-DCM}^{Boost}$ in the form of (4b) using (A1), (A10) and (A16) presented in the Appendix.

(8) Define the custom equation that the curve $Z=f(X,Y)$ should fit into. The custom equation should be (5a) in case of CCM or (5b) in case of DCM at PF=1.

(9) Set initial values to the coefficients c_i or c'_i , $x_{f(pu)}$ and S_b for the fitting algorithm to converge to reasonable results. While S_b together with the nominal AC voltage V_g are known, the rest of the parameters are unknown. However, reasonable technical constraints related to the power switches, filter characteristics, the PVC control method, etc. can be used for the initial estimation of coefficients c_i or c'_i (see the following sub-section and Appendix).

(10) Derive the final expression of P_{total}^{PVC} at PF=1 for specific V_d : The Curve Fitting Tool shall converge to specific values of c_i and/or c'_i .

(11) Derive P_{loss}^{inv} at any P_o and PF \neq 1 using (3).

(12) Substitute $P_{in} = P_{total}^{PVC} + P_o$ either in (4a) or in (4b) depending on the operation mode.

(13) Insert the derived (4a) or (4b) into (5a) or (5b) respectively, Now, the only unknown is P_{total}^{PVC} .

(14) Solve (5):

a) It is noted that (5a) yields a 2nd order equation with respect to $P_{total-CCM}^{PVC}$. Only one of the two solutions leads to technically reasonable results.

b) Eq. (5b) is a 4th order equation with respect to $P_{total-DCM}^{PVC}$. The two out of the four solutions are excluded as technically unreasonable. Out of the two reasonable solutions-which are generally very close- the higher value should be selected since the other one gives losses lower than at PF=1, as it will be shown.

B. Determination of Coefficients following Technical Constraints

Any Curve Fitting Tool needs reasonable initial values as an input (maximum and minimum ones) in order to derive reasonable coefficients in any fitting expression. Each of the unknown coefficients c_i and c'_i in (3) and (4) is a sum of other “sub-coefficients” k_i , $i=1-20$ ((A17) in Appendix). All k_i are functions of several technical parameters the range of which is subject to certain constraints such as the following:

- (i) The actual resistances of the filter inductors, $R_{filter}^{DC/DC}$ and $R_{filter}^{DC/AC}$, are of the order of $m\Omega$, [31] with a minimum value of $10m\Omega$ and a maximum value that is determined by the following rough constraint: the losses on both filters at nominal PVC power should be less than P_{total}^{PVC} at PF=1. The nominal currents in the AC and DC side are derived by the nominal power and the respective voltages. This constraint shall be used in (A1) and (A2) for determining k_1 and k_2 respectively; k_2 is a part of c_3 in (A17.c), while k_1 is a part of c'_7 in (A17.j) and c_7 in (A17.g). Therefore, the maximum values of resistances determine the maximum values of these coefficients.
- (ii) The minimum and maximum value of V_d can be extracted from the PVC datasheet. This constraint is used for the evaluation of the range of c_i, c'_i , for $i \geq 6$.
- (iii) V_{DC-L} has to be higher than the highest V_d the PVC can operate at, and $V_{DC-L} \leq 1kV$; It is used in almost all coefficients k_i, c_i and c'_i .
- (iv) V_g is the nominal grid voltage (per phase value) because the PVC manufacturers provide the efficiency curves at PF=1 for nominal AC voltage. An additional parameter λ is used in this paper to indicate whether the inverter of the PVC is a 3ph or a 1ph one. Hence $\lambda = \sqrt{3}$ for 3ph inverters, while for 1ph ones $\lambda = 1$.
- (v) The number of switches with antiparallel diodes in the inverter can be $N=2$ or 4 for 1ph inverters and $N=6$ for 3ph ones [26]; In the DC/DC converter it is considered to be $N=1$ /MPPT input. The number of MPPT inputs can be taken from the PVC datasheet.
- (vi) As it can be deduced from the datasheets of IGBT and diodes manufacturers [27,28], the on-state, zero-current, collector-emitter voltage, u_{CE0} and the forward voltage u_{F0} are in the range $0.5-2V$. Another constraint is that $u_{CE0} > u_{F0}$, for IGBTs with anti-parallel diodes. The equivalent resistances r_{CE} and r_F are in the range 10 to $100m\Omega$; These parameters are used for the estimation of the range of coefficients, $k_{12}-k_{20}$ with (A14), (A15) and (A16).
- (vii) $x_f(\text{pu}) \leq 0.1\text{pu}$ in order to limit the AC voltage drop during operation, thus enhancing the dynamic response of the PV inverter [30].
- (viii) the switching frequency is usually in the range $5-30kHz$ for both converters composing the PVC [29]; it is used for the estimation of the range of coefficients, k_3-k_{11} with (A4), (A9) and (A10). The maximum value of the switching frequency is also limited by additional constraints on coefficients c_1 and c'_1 mentioned below.
- (ix) the modulation index $m \leq 1$, since over modulation causes excessive harmonic distortion [25];

- (x) Usually, the IGBT and diode manufacturers provide the switching energy losses as a 2nd order function of the current measured at a specific voltage V_{nom} . Therefore, the maximum values of the coefficients α, β , and γ (also defined in Appendix) of the switching losses are $\alpha_{max}=5 \cdot 10^{-4}$, $\beta_{max}=0.05$, and $\gamma_{max}=5$, when the switching energy loss is expressed in mJ [32]. The minimum value of V_{nom} has to be equal to the minimum V_d (information from the datasheet) and its maximum value is up to $1.5kV$, for PVC in LV applications. These parameters are used for the estimation of the range of coefficients, k_3-k_{11} with (A4), (A9) and (A10).
- (xi) Since I_{oBmax} is the maximum boundary current at the DC-link, its minimum value is for maximum $V_{DC-L}=1kV$, thus, $I_{oBmax} \geq S_b/1kV$, while its maximum value is for the lowest V_{DC-L} (in the extreme case it is equal to the highest V_d) and the highest P_{in} taken from (7a), i.e., $I_{oBmax} \leq P_{in,max}/V_{d,max}$. This parameter is used for the estimation of the range of coefficients, $k_6-k_7, k_9-k_{10}, k_{16}$ and k_{19} with (A9), (A10), (A15) and (A16).
- (xii) Coefficients c_1 and c'_1 account for the PVC losses at zero output power. However, the PVC manufacturers provide the efficiency up to a minimum P_o but not at $P_o=0$ as can be noticed in Fig.1. Therefore, their maximum value is set by the losses calculated from the lowest of the efficiency curves provided in the datasheet at the lowest P_o (denoted with red circles in Fig.1). The minimum value of c_1 and c'_1 must be set slightly larger than the PVC standby losses (standby losses appear when the PVC is completely de-energized). A good guess is to set them equal to one fourth of their maximum value.

IV. VALIDATION

The power losses derived with (5a) and (5b) will be validated through simulations and measurements, respectively. The authors had full access to a relatively large PV plant in Greece, the PVC of which operated at DCM. In this plant we could change the PF settings of eight PVCs and make them operate at non-unity PF. For the period of a week we could measure P_{in} and P_o on each of the PVC, thereby calculate their losses. To make some of the PVC operate at CCM would require to reconfigure their PV strings so that they would operate either close to $400V$ or close to $800V$. Such a reconfiguration was not allowed by the PV owners, prohibiting us to evaluate the losses under CCM with field measurements. As the authors do not possess a suitable lab setup to validate the CCM losses experimentally, this validation was done via detailed simulations.

A. Field Measurements – Discontinuous Conduction Mode

In a 1003.52 kW_p PV plant in Central Greece ($39^\circ 36' 52''N$ and $21^\circ 52' 38''E$), fifty-six SMA Sunny Tripower17000TL PVCs have been installed and operate since November 2010 with no RP exchange. In July 2017 eight PVCs were set for a week (15/07 to 23/07) to operate at eight different PFs (four of them at PF=0.8, 0.85, 0.9 and 0.95 in over-excitation mode, while the other four at the same PFs in under-excitation mode). It is noted that we adopted this approach in order to avoid

TABLE I
UPPER & LOWER LIMITS OF COEFFICIENTS c_1 - c_9 AND x_f (pu)

	c'_1	c_2	c_3	c_4	c_5
Lower	15	10^{-3}	10^{-9}	0	-10^{-7}
Upper	50	0.02	10^{-6}	$2 \cdot 10^{-3}$	10^{-7}
	c'_6	c'_7	c'_8	c'_9	x_f (pu)
Lower	10^{-3}	10^{-9}	10^{-3}	$5 \cdot 10^{-7}$	0.01
Upper	0.01	10^{-7}	0.01	10^{-5}	0.1

TABLE II
RESULTS OF CURVE FITTING FOR COEFFICIENTS c_1 - c_5

	0.8/Over	0.8/Under	0.85/Over	0.85/Under
c'_1	27.54	27.54	27.54	32
c_2	0.009	0.0125	0.009	0.0131
c_3	$4 \cdot 10^{-7}$	$5 \cdot 10^{-7}$	$3.9 \cdot 10^{-7}$	$5 \cdot 10^{-7}$
	0.9/Over	0.9/Under	0.95/Over	0.95/Under
c'_1	25	27	27	27
c_2	0.001	0.0125	0.0113	0.0125
c_3	$5.6 \cdot 10^{-7}$	$5 \cdot 10^{-7}$	$4 \cdot 10^{-7}$	$4 \cdot 10^{-7}$

violating the grid code imposed by the Greek Distribution System Operator that demands all PV plants to operate at unity PF at their point of common coupling with the distribution grid. For the same eight PVCs, measurements of losses were taken also during the previous week (07/07-14/07) when they operated at PF=1. The PVC losses were measured by monitoring (every 10min) their power at the DC and AC side.

Simultaneously, their PF was measured to test whether it was equal with the set value. Although the eight PVCs are of the same type, they actually differ by some small manufacturing details and operate at slightly different PV voltages ($V_d \sim 550$ -565 V) and local ambient temperature conditions. For these reasons, instead of using the efficiency curve for 600V shown in Fig. 1(a), their actual efficiency curve for PF=1 was measured. These eight efficiency curves were found to be very close (although not exactly) to the one shown in Fig.1(a) for 600V.

This fact implies that the respective boost converters operated at DCM. Therefore, (5b) will be validated through the following measurements. The next step was the estimation of coefficients $c_i, c'_i, (i = 1 - 9)$ in (5b) by inserting more than 300 measured values of $(P_o, P_{in}, P_{total-DCM}^{PVC})$ in MATLAB Curve Fitting Tool. The version of MATLAB that has been used is: R2017a, 64bit running on a 16GB RAM, Core i7-6700, 2.6GHz computer. Setting the technical constraints described in Section III.B and equations (A1-A17), the range of the sub-coefficients k_i and subsequently of the coefficients c'_i and $c_i, (i = 1 - 9)$ at DCM were estimated as shown in Table I. These upper and lower limits were given as initial conditions in the Curve Fitting Tool which converged in the estimation of the final c'_i and $c_i, (i = 1 - 9)$ with the Non-Linear Least Squares method (MaxFunEvals:3000, MaxIter:3000) in about 5 seconds. Most coefficients derived from the Curve Fitting Tool had the same value for each of the eight PVCs, i.e., x_f (pu) = 0.033 pu, $c_4 = -2 \cdot 10^{-3}$, $c_5 = 10^{-7}$, $c_6 = 0.01$, $c_7 = 6.76 \cdot 10^{-8}$, $c_8 = 10^{-3}$ and $c_9 = 10^{-5}$. The rest of the coefficients appear in Table II and show small differences among the eight PVCs due to the different operating conditions mentioned before.

The final step was to evaluate the PVC losses via (5b) using the derived coefficients and compare the results with the actual

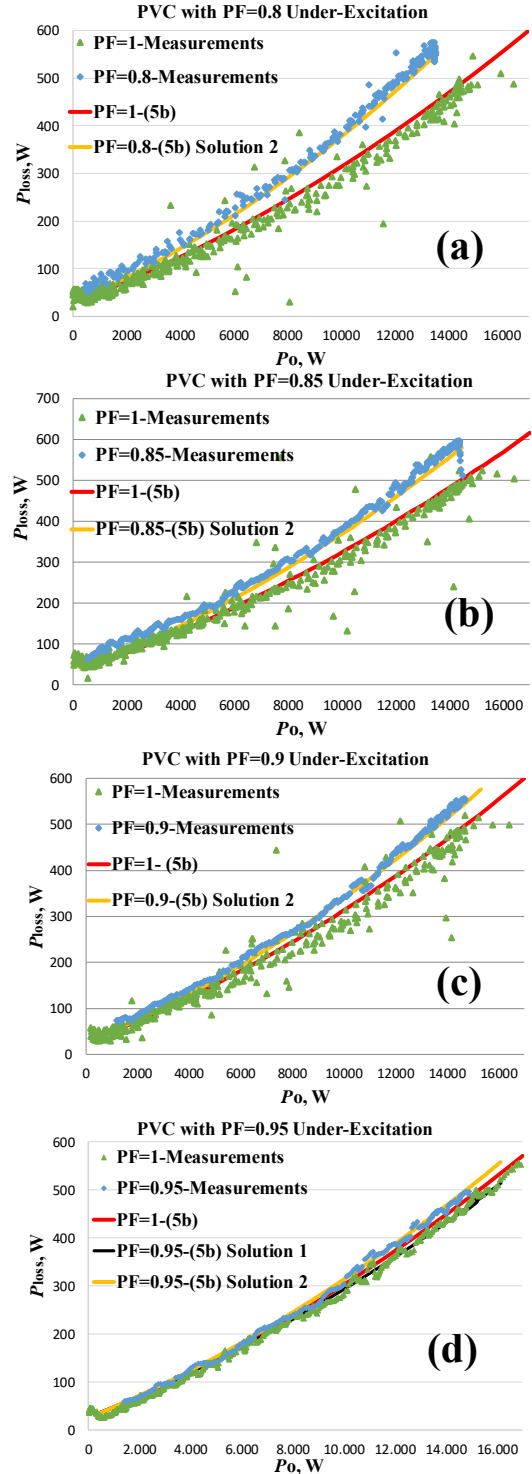


Fig. 5. Measurements and calculations of losses of 4 PVCs at PF=1 and various PFs in Under-excitation mode.

measurements of the PVC losses for the eight different PFs. This is shown in Fig. 5 for the cases of under-excitation and in Fig. 6 for the cases of over-excitation. The good convergence of calculations by (5b) and measurements validates the proposed methodology in the case of DCM.

As mentioned before, (5b) yields two solutions. The second solution (depicted as Solution 1) also appears in Fig. 5(d) and 6(d) with black solid line. This solution is technically

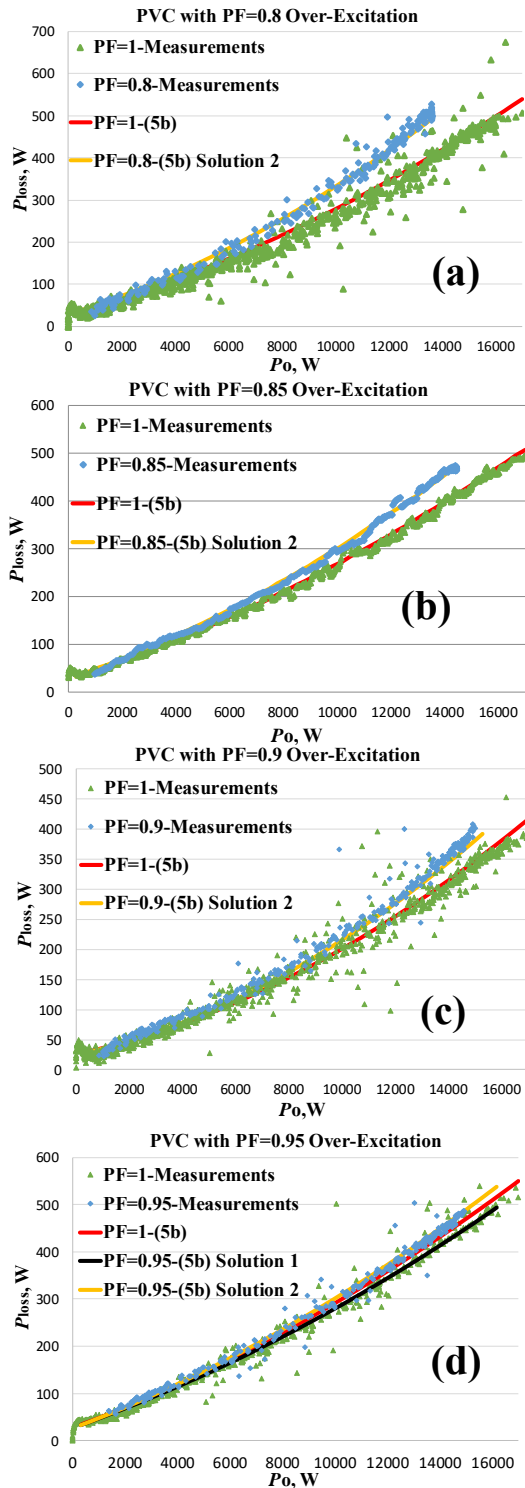


Fig. 6. Measurements and calculations of losses of 4 PVCs at PF=1 and various PFs in Over-excitation mode.

unacceptable because it estimates losses at PF=0.95 smaller than in the case with PF=1.

B. Simulations-Continuous Conduction Mode

In order to have the same basis in all the validation cases and to derive a rather realistic simulation model, we tried to simulate the SMA Tripower 17kVA converter. The simulation

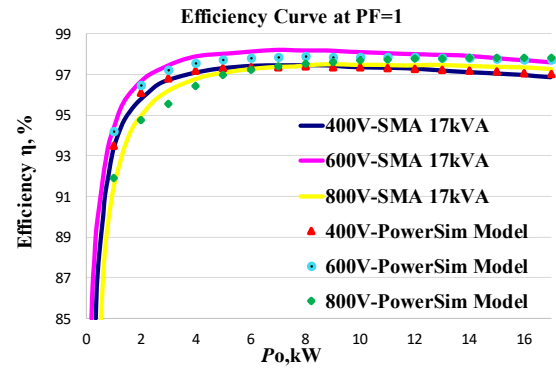


Fig. 7 Comparison of efficiency curves (simulation results and manufacturer's data)

TABLE III
HARDWARE PARAMETERS OF THE SIMULATION MODEL

DC/DC boost converter					
$R_{filter}^{DC/DC}$	50mΩ	r_{CE}	30mΩ	u_{CE0}	1.5V
u_{F0}	0.8V	r_F	12.5mΩ	V_{nom}	900V
α_{sw}^{off}	$10^{-6}J$	β_{sw}^{off}	$10^{-6}J$	γ_{sw}^{off}	$2 \cdot 10^{-3}J$
α_{sw}^{on}	$1.2 \cdot 10^{-6}J$	β_{sw}^{on}	$2.5 \cdot 10^{-5}J$	γ_{sw}^{on}	$5.3 \cdot 10^{-3}J$
Inverter					
u_{CE0}	1,1V	r_{CE}	30mΩ	V_{nom}	600V
u_{F0}	0,8V	r_F	10mΩ	V_g	$400/\sqrt{3} V$
α_{sw}^{off}	0	β_{sw}^{off}	$3.69 \cdot 10^{-5}J$	γ_{sw}^{off}	$7.63 \cdot 10^{-4}J$
α_{sw}^{on}	$2 \cdot 10^{-7}J$	β_{sw}^{on}	$1.93 \cdot 10^{-5}J$	γ_{sw}^{on}	$1.08 \cdot 10^{-4}J$
λ	$\sqrt{3}$	w	$0.5 \cdot \sqrt{3/2}$		

was carried out with the PSIM software, in particular using its Thermal Module that allows the detailed simulation of the conduction and switching losses. Using as input the maximum power rating of the converter, suitable switches (IGBTs and diodes) have been selected from the database of IXYS company [33, 34]. The aim was to build a model that would simulate as accurately as possible the operating conditions described in the respective manufacturer leaflet [15] and yield almost the same efficiency curves for PF=1 and for the three PV voltages (400, 600 and 800V). Then, using the Thermal Module option of the simulation software, the losses could be estimated at various non-unity PFs. These losses are then compared to the losses derived using the proposed methodology, i.e., using (3) and (4a) after estimating the coefficients c_1-c_7 in them based only on the data from the efficiency curve at PF=1.

The boost converter has been designed in the simulation model, so that: it has 99% efficiency at 17kW; its DC voltage ripple does not exceed 1%; it is in CCM for $V_d = 800V$ and $P_o = 1-17kW$; it is in DCM at 600V for $P_o = 1-17kW$; it is near the boundary condition at 400V and $P_o = 16kW$. The above conditions lead to the selection of $V_{DC-L} = 830V$. The selected inductor, capacitor and switching frequency are 186μH, 781μF and 13 kHz. Other parameters of the boost converter hardware are shown in Table III.

The inverter has been designed as a 3ph, H-6 full bridge with an LC filter ($L_f = 1mH$, $C_f = 5.5\mu F$, $R_{filter}^{DC/AC} = 12.4m\Omega$ –EMC filter found in [31]). The six IGBTs with their antiparallel diodes were modelled with parameters from [35]. Other parameters of the inverter hardware are shown in Table III. The

TABLE IV

UPPER & LOWER LIMITS OF COEFFICIENTS c_1 , c_6 AND c_7 FOR CCM

	c_1	c_6	c_7
Lower	15	$6.25 \cdot 10^{-4}$	$4 \cdot 10^{-8}$
Upper	120	$7.5 \cdot 10^{-3}$	$6.56 \cdot 10^{-7}$

TABLE V

ACTUAL & ESTIMATED COEFFICIENTS c_1 - c_7 AND X_i (PU)

	c_1	c_2	c_3	c_4
Actual	120	$6.73 \cdot 10^{-3}$	$2.2 \cdot 10^{-7}$	$6.26 \cdot 10^{-4}$
Estimated	115	$5.8 \cdot 10^{-3}$	$2.5 \cdot 10^{-7}$	$5.5 \cdot 10^{-4}$
	c_5	c_6	c_7	X_i (pu)
Actual	$1.36 \cdot 10^{-8}$	$2.25 \cdot 10^{-3}$	$1.38 \cdot 10^{-7}$	0.034
Estimated	$2 \cdot 10^{-8}$	$2.95 \cdot 10^{-3}$	$1.2 \cdot 10^{-7}$	0.03

inverter is controlled as a Current-Controlled Voltage Source [25] with $f_{sw}^{inv}=10$ kHz. The operating junction temperature of the various switches was set to 125°C.

Running the simulation model for PF=1, $P_o=1-17$ kW and $V_d=400, 600$ and 800V, all losses (conduction, switching, and filter) were calculated. The respective efficiency curves are shown in Fig. 7 together with the curves provided by the manufacturer for the same conditions. The good fitting implies that the simulation model is quite realistic. An estimation of the good fitting can be made through the Root-Mean-Squared-Error (RMSE) which was evaluated to be: 0.14 for the 400V curves, 0.20 for the 600V curves and 0.24 for the 800V curves if the efficiency is expressed in percent as in Fig. 7. Then, the simulation model was run at $V_d=800$ V for PF=0.8 and 0.9 in over-excitation and under-excitation mode for the whole range of P_o . The losses on the PVC are shown in Fig. 8(a) and Fig. 8(b) with dots.

Next, the coefficients $c_i, (i = 1 - 7)$ in (3) and (4a) were evaluated using 50 values from the 800V curve of Fig. 7 and the procedure described in Section III with upper and lower limits of Table IV for c_1, c_6 and c_7 and with upper and lower limits of Table I for $c_2 - c_5$. Finally, using (5a) with the derived coefficients, the PVC losses were calculated for the same PFs as shown in Fig. 8(a) and Fig. 8(b) with solid lines. The very good fitting implies that the proposed methodology is valid also for the cases of CCM, in two-stage PVCs.

The effectiveness of the proposed methodology can also be demonstrated with the evaluation of the coefficients c_1 - c_7 in (3) and (4a). In the case of detailed simulation all hardware parameters are known as shown in Table V. Therefore, the coefficients c_1 - c_7 can be calculated following the equations in Appendix. The calculated coefficients are shown in Table V as "actual". The same coefficients are estimated following the proposed fitting methodology and are also shown in Table V as "estimated". It can be observed that the proposed methodology can make very good estimation of the coefficients for two-stage PVC with boost DC/DC converters provided that a sufficient number of data points from the efficiency curve at PF=1 are available and reasonable technical constraints are given for the range of some parameters.

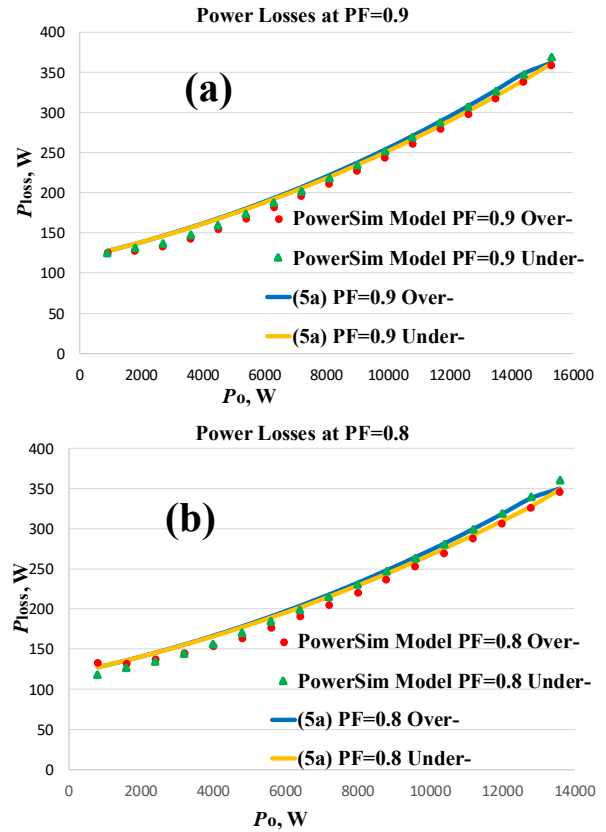


Fig. 8 Comparison of converter losses at four PFs (simulation results and results derived by (5a)): (a) at PF=0.9 and (b) at PF=0.8.

TABLE VI
EXAMPLE OF PVC OPERATING MODE

% of time	3	6	13	10	48	20
% of rated power	5	10	20	30	50	100
η (%) under PF=1	93	96.2	97.7	98	98.1	97.6
PF (Under-Excit)	1	1	0.98	0.95	0.85	0.8
η (%) under PF \neq 1	93	96.2	97.5	97	96.7	96.2

V. CONCLUSIONS AND DISCUSSION

An analytical method for estimating the power losses of two-stage PVCs with non-isolated DC/DC boost converter under RP provision has been derived and tested against simulations and field measurements with very good accuracy.

The presented method is based on basic operating principles of the power converter theory and on the efficiency curve at PF=1 given by the manufacturers, without requiring detailed knowledge of the involved hardware parameters or even the level of DC-link voltage. The analytical expressions of the losses and their separation have been validated for the specific type of PVCs, i.e. string PVC, with DC/DC boost converter and 3-phase, H-6 bridge inverter. It is shown that for a certain range of commonly used PV voltages the involved boost DC/DC converter operates at DCM for almost all power range, thereby with increased efficiency. This feature explains why the PVC manufacturers prefer this type of DC/DC converter for 3-phase PVCs of small to medium size (1-50 kVA). A method for deciding whether the PVC operates at DCM or CCM has also

been suggested. The proposed methodology can be useful for the following reasons:

- (i) currently the PVC manufacturers do not provide data on the losses when the converter operates at $PF \neq 1$ because, until, now these converters were required to operate only at $PF=1$,
- (ii) it is expected that in the near future, the converters will be required to provide RP as an AS. It is evident that this AS must be quantified in order to be remunerated. Knowing the additional losses incurred on the converter when providing RP is equivalent to knowing its additional operational cost. The following example serves as clarification of the above assertions: Let us assume the 17kVA PVC operating under Central European conditions as shown in Table VI. In case it operates with $PF=1$, the energy that will inject into the grid is 25.1 MWh assuming 3000h/year of equivalent clear days. In case it operates with PFs as shown in row 4 of Table VI, the energy that would be injected is 22.8 MWh. This difference of 2.3MWh/year is the operational cost –in terms of energy- of the PVC for providing RP to the grid.
- (iii) Although the proposed methodology was validated concerning specific PVC topologies, the presented theoretical background together with the idea of separating the individual losses among the components of the PVC that are affected or not by the RP, can be used by researchers and design engineers for other topologies as well.
- (iv) Additionally, as pointed out with the technical literature review in Section I, measurements of PVC losses, when they exchange RP have been taken so far only in lab environment. This paper presents measurements of PVC losses taken in a real 1MW_p PV plant. Important is also the fact that the measurements were taken for the same type of PVCs, making them operate at different PFs at the same time with the same ambient conditions for one week. Exactly the same eight PVCs were also monitored with respect to their losses, one week earlier while operating under $PF=1$. The authors believe that such a measurement setup makes the comparison of the losses under various PFs more solid.

VI. APPENDIX

The losses on the DC/DC converter will be expressed as a function of the input DC current $I_d = P_{in}/V_d$ while the losses on the inverter as a function of the output AC current- either RMS $I_{o,AC} = P_o/(V_g \cdot PF \cdot \lambda)$ or peak $i_p = I_{o,AC} \cdot \sqrt{2}$, where V_g is the ac output phase voltage. The additional parameter λ is used in this paper to indicate whether the inverter of the PVC is a 3ph or a 1ph one. Hence $\lambda = \sqrt{3}$ for 3ph inverters, while for 1ph ones $\lambda = 1$. The losses on the switches (IGBTs and diodes) and the losses on the filter inductors are considered. The IGBT and diode losses can be divided in three groups [27]: conduction, switching and blocking (leakage) losses with the latter being negligible.

For given V_d the ohmic losses on the DC/DC converter

inductor can be expressed as a function of I_d , and P_{in}

$$P_{loss,filter}^{boost} = R_{filter}^{DC/DC} \cdot I_d^2 = \frac{R_{filter}^{DC/DC} \cdot P_{in}^2}{V_d^2} = k_1 \frac{P_{in}^2}{V_d^2} \quad (A1)$$

where $R_{filter}^{DC/DC}$ is the ohmic resistance of the filter. The ohmic losses on the DC/AC inverter inductor can be expressed as a 2nd order function of I_o , and P_o

$$P_{loss,filter}^{inv} = \lambda^2 \cdot R_{filter}^{DC/AC} \cdot I_{o,AC}^2 = \frac{R_{filter}^{DC/AC}}{V_g^2} \cdot \frac{P_o^2}{PF^2} = k_2 \frac{P_o^2}{PF^2} \quad (A2)$$

where $R_{filter}^{DC/AC}$ is the ohmic resistance of the inverter filter.

The turn-on $E_{sw}^{IGBT/on}$ and turn-off energy losses, $E_{sw}^{IGBT/off}$ of the IGBTs are provided by the manufacturers for a specific DC voltage level. They are usually a 2nd order function [28] of the collector current (I_c). The diodes have turn-off energy losses (reverse-recovery energy) E_{rec}^{diode} , while their switch-on energy losses are negligible [27]. The diodes' losses are usually a 2nd order function of the diode's forward current (I_F) for a specific DC voltage, as it can be seen in many diodes' datasheets. Within certain limits, the dependence on the DC voltage can be assumed to be linear [28], therefore,

$$\begin{aligned} E_{sw}^{IGBT-on} &= \left(\gamma_x^{sw/on} + \beta_x^{sw/on} \cdot I_c + \alpha_x^{sw/on} \cdot I_c^2 \right) \cdot \frac{V_{DC-L}}{V_{nom}} \\ E_{sw}^{IGBT-off} &= \left(\gamma_x^{sw/off} + \beta_x^{sw/off} \cdot I_c + \alpha_x^{sw/off} \cdot I_c^2 \right) \cdot \frac{V_{DC-L}}{V_{nom}} \\ E_{rec}^{diode} &= \left(\gamma_x^{dio} + \beta_x^{dio} \cdot I_F + \alpha_x^{dio} \cdot I_F^2 \right) \cdot \frac{V_{DC-L}}{V_{nom}} \end{aligned} \quad (A3)$$

where V_{nom} is the DC voltage for which the switching energies are given, while V_{DC-L} is the DC-link voltage that is actually applied on the switch or diode. The coefficients α , β , γ are provided by the switch manufacturer, while subscript x refers to either the inverter ($x=1$) or DC/DC converter ($x=2$). In the inverter, the currents I_c and I_F in (A3) are the instantaneous values of $i_p \cdot \sin(2\pi t/T_o)$. It is noted that the IGBTs and diodes conduct over half period ($T_o/2$). The average switching power losses are calculated by the switching energies over a period T_o of the output frequency (50 or 60Hz) multiplied with the switching frequency f_{sw}^{inv} [28]. Therefore, the total switching losses can be expressed as

$$\begin{aligned} P_{sw}^{inv} &= N \cdot f_{sw}^{inv} \cdot \frac{V_{DC-L}}{V_{nom}} \cdot \left[\frac{1}{2} \left(\gamma_1^{dio} + \gamma_1^{sw/on} + \gamma_1^{sw/off} \right) + \right. \\ &\quad \left. + \left(\beta_1^{dio} + \beta_1^{sw/on} + \beta_1^{sw/off} \right) \cdot \frac{i_p}{\pi} + \right. \\ &\quad \left. + \frac{i_p^2}{4} \cdot \left(\alpha_1^{dio} + \alpha_1^{sw/on} + \alpha_1^{sw/off} \right) \right] = \\ &= k_3 + k_4 \frac{P_o}{PF} + k_5 \frac{P_o^2}{PF^2} \quad \text{under} \end{aligned} \quad (A4)$$

$$k_3 = N \cdot f_{sw}^{inv} \cdot \frac{V_{DC-L}}{V_{nom}} \cdot \frac{1}{2} \cdot \left(\gamma_1^{dio} + \gamma_1^{sw/on} + \gamma_1^{sw/off} \right)$$

$$k_4 = \frac{\sqrt{2} N \cdot f_{sw}^{inv}}{\lambda V_g \pi} \cdot \frac{V_{DC-L}}{V_{nom}} \cdot \left(\beta_1^{dio} + \beta_1^{sw/on} + \beta_1^{sw/off} \right)$$

$$k_5 = \frac{N \cdot f_{sw}^{inv}}{2 \lambda^2 V_g^2} \cdot \frac{V_{DC-L}}{V_{nom}} \cdot \left(\alpha_1^{dio} + \alpha_1^{sw/on} + \alpha_1^{sw/off} \right)$$

In the DC/DC converter, the instantaneous switch current is

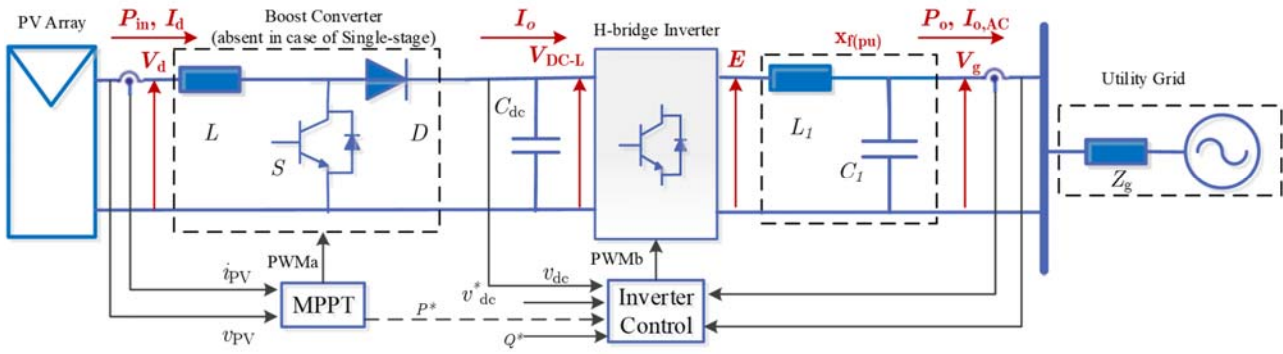


Fig. A1. Simplified single-phase diagram of a grid-connected PVC.

$I_C = i_{sw,min} = i_{L,min}$ for $E_{sw}^{IGBT/on}$ (i_L is the inductor current), while $I_C = i_{sw,max} = i_{L,max}$ for $E_{sw}^{IGBT/off}$. For the diode, $I_F = i_{L,max}$ for the calculation of E_{rec}^{diode} . Therefore, the aggregated switching losses for a DC/DC converter can be described by

$$P_{sw}^{boost} = f_{sw}^{boost} \cdot \frac{V_d}{V_{nom}} \cdot \left[\begin{aligned} & \left(\gamma_2^{dio} + \gamma_2^{sw/off} + \gamma_2^{sw/on} \right) + \\ & \left(\alpha_2^{dio} + \alpha_2^{sw/off} \right) i_{L,max}^2 + \alpha_2^{sw/on} i_{L,min}^2 + \\ & + \beta_2^{sw/on} \cdot i_{L,min} + \left(\beta_2^{dio} + \beta_2^{sw/off} \right) \cdot i_{L,max} \end{aligned} \right] \quad (A5)$$

If ΔI_L is the inductor current ripple, and f_{sw}^{boost} the switching frequency, it can be proved that,

$$\left. \begin{aligned} i_{L,max} - i_{L,min} &= \Delta I_L = \frac{V_d \cdot D}{L \cdot f_{sw}^{boost}} \\ L \cdot f_{sw}^{boost} &= \frac{2}{27} \frac{V_{DC-L}}{I_{oB,max}} \end{aligned} \right\} \Rightarrow \Delta I_L = \frac{27}{2} \frac{V_d \cdot I_{oB,max} \cdot D}{V_{DC-L}} \quad (A6)$$

In CCM the duty cycle D remains constant at $1 - V_d/V_{DC-L}$, while $i_{L,max} = I_d + 0.5\Delta I_L$, $i_{L,min} = I_d - 0.5\Delta I_L$, thus

$$\Delta I_L = \frac{27}{2} \frac{V_d \cdot I_{oB,max}}{V_{DC-L}^2} (V_{DC-L} - V_d) \quad (A7)$$

In DCM, $i_{L,max} = \Delta I_L$ and $i_{L,min} = 0$ and the duty-cycle D depends on P_{in} ,

$$D = \sqrt{\frac{4}{27} \frac{(V_{DC-L} - V_d)}{V_d^2} \frac{P_{in}}{I_{oB,max}}} \Rightarrow \Delta I_L = \frac{3}{V_{DC-L}} \sqrt{3 I_{oB,max} (V_{DC-L} - V_d) \cdot P_{in}} \quad (A8)$$

Since in the CCM, $I_{oB,max}$, V_{DC-L} and V_d can be assumed to remain constant, it can be proved using (A5)-(A7) that the switching losses can be expressed as 2nd order function of P_{in}

$$P_{sw}^{boost} = k_6 + k_7 P_{in} + k_8 P_{in}^2 \quad \text{with} \quad (A9)$$

$$k_6 = f_{sw}^{boost} \cdot \frac{V_d}{V_{nom}} \cdot \left[\begin{aligned} & \left(\gamma_2^{dio} + \gamma_2^{sw/off} + \gamma_2^{sw/on} \right) + \\ & + \left(\beta_2^{dio} + \beta_2^{sw/off} - \beta_2^{sw/on} \right) \cdot 0.5\Delta I_L + \\ & + 0.25 \left(\Delta I_L \right)^2 \cdot \left(\alpha_2^{dio} + \alpha_2^{sw/off} + \alpha_2^{sw/on} \right) \end{aligned} \right]$$

$$k_7 = f_{sw}^{boost} \cdot \frac{V_d}{V_{nom}} \cdot \left[\begin{aligned} & \Delta I_L \left(\alpha_2^{dio} + \alpha_2^{sw/off} - \alpha_2^{sw/on} \right) \\ & + \left(\beta_2^{dio} + \beta_2^{sw/off} + \beta_2^{sw/on} \right) \end{aligned} \right]$$

$$k_8 = f_{sw}^{boost} \cdot \frac{V_d}{V_{nom}} \cdot \left(\alpha_2^{dio} + \alpha_2^{sw/off} + \alpha_2^{sw/on} \right)$$

In the DCM using (A5), (A6) and (A8) the switching losses are in the form of

$$P_{sw}^{boost} = k_9 P_{in} + k_{10} \cdot \sqrt{P_{in}} + k_{11} \quad \text{with} \quad (A10)$$

$$k_9 = f_{sw}^{boost} \cdot \frac{V_d}{V_{nom}} \left(\alpha_2^{dio} + \alpha_2^{sw/off} \right) \frac{27 I_{oB,max} (V_{DC-L} - V_d)}{V_{DC-L}^2}$$

$$k_{10} = \frac{3 f_{sw}^{boost}}{V_{DC-L}} \frac{V_d}{V_{nom}} \left(\beta_2^{dio} + \beta_2^{sw/off} \right) \sqrt{3 I_{oB,max} (V_{DC-L} - V_d)}$$

$$k_{11} = f_{sw}^{boost} \cdot \frac{V_d}{V_{nom}} \cdot \left(\gamma_2^{dio} + \gamma_2^{sw/off} \right)$$

The conduction losses in both converters, appear on the IGBTs and the diodes. IGBT conduction losses [27] can be calculated using an IGBT approximation with a series connection of DC voltage source (u_{CE0}) representing the IGBT on-state, zero-current, collector-emitter voltage and a collector-emitter on-state resistance (r_{CE}). The same approximation can be used for the diodes with u_{F0} being the forward voltage and r_F the forward resistance. Therefore, the conduction losses of either the IGBT or the diode (denoted as x below) over a switching period T_{sw} can be expressed as

$$P_{cond}^x = \frac{1}{T_{sw}} \int_0^{T_{sw}} p_{cond}^x(t) dt = V_{x,0} \cdot I_x^{av} + r_x \cdot \left(I_x^{rms} \right)^2 \quad (A11)$$

In the inverter, the IGBTs conduct over $T_0/2$ while the diodes for the other $T_0/2$. In the PWM pattern, the duty cycle varies within T_0 . If the phase angle is φ ($PF = \cos\varphi$) and the output voltage is $\sqrt{2}V_g \cdot \sin\left(\frac{2\pi}{T_0}t + \varphi\right)$, it can be proved [25,28] that the losses on the IGBT and diode can be expressed as function of i_p

$$P_{cond}^{IGBT} = i_p \cdot \left[\frac{1}{2} \cdot \left(\frac{u_{CE0}}{\pi} + r_{ce} \frac{i_p}{4} \right) + m \cdot PF \cdot \left(\frac{u_{CE0}}{8} + r_{ce} \frac{i_p}{3\pi} \right) \right] \quad (A12)$$

$$P_{cond}^{diode} = i_p \cdot \left[\frac{1}{2} \cdot \left(\frac{u_{F0}}{\pi} + r_F \frac{i_p}{4} \right) - m \cdot PF \cdot \left(\frac{u_{F0}}{8} + r_F \frac{i_p}{3\pi} \right) \right]$$

If $\bar{E} \angle \delta^\circ$ and $\bar{V}_g \angle 0^\circ$ are the voltages across the inverter output filter reactance X_f , the modulation index ($m \leq 1$) can be expressed as

$$\left. \begin{aligned} P_o &= \frac{E \cdot (\lambda \cdot V_g)}{X_f} \sin \delta \\ P_o \cdot \tan \varphi &= \frac{(\lambda \cdot V_g)}{X_f} (E \cos \delta - \lambda \cdot V_g) \\ E &= w \cdot m \cdot V_{DC-L} \\ X_f &= x_{f(pu)} \cdot \frac{(\lambda \cdot V_g)^2}{S_b} \end{aligned} \right\} \Rightarrow \quad (A13)$$

$$\Rightarrow m = \frac{\lambda \cdot V_g}{w \cdot V_{DC-L}} \sqrt{\left(\frac{x_{f(pu)} \cdot P_o}{S_b} \right)^2 + \left(\frac{x_{f(pu)} \cdot P_o \tan \varphi}{S_b} + 1 \right)^2}$$

where S_b is the nominal PVC AC apparent power while $w = 0.5 \cdot \sqrt{3/2}$ for 3ph inverters and $w = 0.5 \cdot \sqrt{2}$ for 1ph inverters, while λ has been defined above [25]. Using (A12)-(A13) the conduction losses for one IGBT with its anti-parallel diode are given in (A14). In the boost converter the average currents are $I_{diode}^{av} = I_{DC-L} = \frac{P_{in}}{V_{DC-L}}$ and $I_{sw}^{av} = P_{in} \cdot (V_{DC-L} - V_d) / (V_{DC-L} \cdot V_d)$. These values are independent of the conduction mode, however, the latter affects the RMS currents, because the conduction periods differ.

$$P_{cond}^{tot} = k_{12} \cdot \frac{P_o}{PF} + k_{13} \cdot \frac{P_o^2}{PF^2} + P_o \cdot \left(k_{14} + k_{15} \cdot \frac{P_o}{PF} \right) \cdot \sqrt{\left(\frac{x_{f(pu)} \cdot P_o}{S_b} \right)^2 + \left(\frac{x_{f(pu)} \cdot P_o \tan \varphi}{S_b} + 1 \right)^2} \quad \text{with} \quad (A14)$$

$$k_{12} = \frac{\sqrt{2} \cdot (u_{CE0} + u_{F0})}{2\pi \lambda \cdot V_g}$$

$$k_{13} = \frac{(r_{ce} + r_f)}{4\lambda^2 \cdot V_g^2}$$

$$k_{14} = \frac{\sqrt{2} \cdot (u_{CE0} - u_{F0})}{8 \cdot w \cdot V_{DC-L}}$$

$$k_{15} = \frac{2 \cdot (r_{ce} - r_f)}{3\pi \lambda \cdot V_g \cdot w \cdot V_{DC-L}}$$

Based on basic power electronic principles and after some mathematical manipulations it can be proved that for the CCM

$$P_{cond}^{boost} = k_{16} + k_{17} P_{in} + k_{18} P_{in}^2 \quad \text{with} \quad (A15)$$

$$k_{16} = \frac{243}{16} \cdot \frac{I_{oB,max}^2 V_d^2 \cdot (V_{DC-L} - V_d)^2}{V_{DC-L}^5} \cdot [r_f V_d + r_{ce} (V_{DC-L} - V_d)]$$

$$k_{17} = \frac{1}{V_{DC-L}} \left[u_{F0} + \frac{u_{CE0}}{V_d} (V_{DC-L} - V_d) \right]$$

$$k_{18} = \frac{1}{V_{DC-L} V_d^2} \cdot [r_f V_d + r_{ce} (V_{DC-L} - V_d)]$$

while for the DCM the form is different

$$P_{cond}^{boost} = P_{in} \left(k_{19} \sqrt{P_{in}} + k_{20} \right) \quad \text{with} \quad (A16)$$

$$k_{19} = \frac{2}{V_{DC-L}^2 V_d} \sqrt{3 I_{oB,max}^2 \cdot (V_{DC-L} - V_d)} \cdot [r_f V_d + r_{ce} (V_{DC-L} - V_d)]$$

$$k_{20} = \frac{1}{V_{DC-L} V_d} [V_d u_{F0} + u_{CE0} (V_{DC-L} - V_d)]$$

By defining:

$$\begin{aligned} c_1 &= k_3 + k_6 + k_{16} & (a) \\ c_2 &= k_4 + k_{12} & (b) \\ c_3 &= k_2 + k_5 + k_{13} & (c) \\ c_4 &= k_{14} & (d) \\ c_5 &= k_{15} & (e) \\ c_6 &= k_7 + k_{17} & (f) \\ c_7 &= k_1 + k_8 + k_{18} & (g) \\ c'_1 &= k_3 + k_{11} & (h) \\ c'_6 &= k_9 + k_{20} & (i) \\ c'_7 &= k_1 & (j) \\ c'_8 &= k_{10} & (k) \\ c'_9 &= k_{19} & (l) \end{aligned} \quad (A17)$$

(5a) and (5b) are derived.

An alternative way to express the losses on the PVC could be via the conventional average switching cycle loss model [39], [40]. According to this model the switching losses are expressed as a function of the average switch current, the reverse recovery charge, Q_{rr} , and the reverse recovery time t_{rr} in order to express the switch-off losses of diodes. Both Q_{rr} and t_{rr} are given in the datasheets of the switch manufacturers as function of the switch forward current (usually a 2nd order function together with the switching energy/recovery losses), [28], [32], [35]. If Q_{rr} and t_{rr} are expressed as functions of the switch current and eventually as function of the power (either P_{in} or P_o depending on the converter type), expressions similar to (A4), (A9) and (A10) can be derived, although with different respective coefficients. This implies that the proper range of these new coefficients should be defined for the proposed model to converge. Regarding the conduction losses, the conventional average switching cycle loss model does not differ from the approach presented in this paper. Therefore, expressions similar to (A14)-(A16) can be derived if the average switch current is expressed as function of P_{in} or P_o .

It is noted that the dependencies of Q_{rr} and t_{rr} on the switch current have already been incorporated in the values of the switching energy losses provided by the switch manufacturers. Therefore, expressions like (A3) are more accurate and additionally relate more directly the switching losses with the power of the converter. This is the reason why they have been preferred in this paper for deriving the analytical expressions of the switching losses instead of the average switching cycle loss model.

VII. REFERENCES

- [1] M. Mejbau Haque, Peter Wolfs, "A review of high PV penetrations in LV distribution networks: Present status, impacts and mitigation measures", *Renew. Sust. Energ. Rev.*, vol. 62, pp. 1195–1208, 2016.
- [2] M. Karimi, H. Mokhlis, K. Naidu, S. Uddin, A.H.A. Bakar "Photovoltaic penetration issues and impacts in distribution network – A review", *Renew. Sust. Energ. Rev.*, vol. 53, pp. 594–605, 2016.
- [3] T. Stetz, F. Marten, and M. Braun, "Improved Low Voltage Grid-Integration of Photovoltaic Systems in Germany", *IEEE Trans. Sustainable Energy*, vol. 4, no. 2, pp. 534–542, Apr. 2013
- [4] H. E. Farag, E. F. El-Saadany and R. Seethapathy, "A Two Ways Communication-Based Distributed Control for Voltage Regulation in Smart Distribution Feeders," *IEEE Trans. Smart Grid*, vol. 3, no. 1, pp. 271–281, 2012.
- [5] B. A. Robbins, C. N. Hadjicostis and A. D. Domínguez-García, "A Two-Stage Distributed Architecture for Voltage Control in Power Distribution Systems," *IEEE Trans. Power Systems*, vol. 28, no. 2, pp. 1470–1482, 2013.

- [6] H. G. Yeh, D. F. Gayme and S. H. Low, "Adaptive VAR Control for Distribution Circuits With Photovoltaic Generators," *IEEE Trans. Power Systems*, vol. 27, no. 3, pp. 1656-1663, Aug. 2012
- [7] R. Bründlinger (AIT Austrian Institute of Technology), "Grid Codes in Europe for Low and Medium Voltage," *6th International Conference on Integration of Renewable and Distributed Energy Resources*, Kyoto, Germany, Nov. 2014, pp. 1-28.
- [8] F. Kalverkamp, B. Schowe-von der Brölie, T. D. Nguyen, T. Mertens and M. Meuser, "Comparative analysis of European Grid Codes and compliance standards for distributed power generation plants with respect to future requirements of," *International ETG Congress 2015; Die Energiewende - Blueprints for the new energy age*, Bonn, Germany, 2015, pp. 1-6.
- [9] E. Demirok, P.C. Gonzalez, K. Frederiksen, D. Sera, P. Rodriguez and R. Teodorescu, "Local Reactive Power Control Methods for Overvoltage Prevention of Distributed Solar Inverters in Low-Voltage Grids", *IEEE Journal of Photovoltaics*, vol. 1, no. 2, pp. 174-182, Dec. 2011.
- [10] V. Calderaro, V. Galdi, F. Lamberti, and A. Piccolo, "A smart strategy for voltage control ancillary service in distribution networks," *IEEE Trans. Power Syst.*, vol. 30, no. 1, pp. 494-502, Jan. 2015.
- [11] S. Weckx, C. Gonzalez, and J. Driesen, "Combined Central and Local Active and Reactive Power Control of PV Inverters", *IEEE Trans. Sustainable Energy*, vol. 5, no. 3, pp.776-784, Jul. 2014.
- [12] C. S. Demoulias, "A new simple analytical method for calculating the optimum inverter size in grid-connected PV plants", *Electric Power Systems Research*, vol. 80, no.10, pp. 1197-1204, 2010.
- [13] S. Ruestera, S. Schwenen, Carlos Batlle and Ignacio Pérez-Arriaga, "From distribution networks to smart distribution systems: Rethinking the regulation of European electricity DSOs," *Utilities Policy*, vol. 31, pp. 229-237, 2014.
- [14] REserviceS Project, "Ancillary services: technical specifications, system needs and costs. Deliverable D 2.2", Nov. 2012.
- [15] Product catalogue for SMA String PV Inverters [Online] Available: http://www.gehrlicher.com/fileadmin/content/pdfs/en/wechselrichter/SMA_Tr_ipower_en.pdf
- [16] SMA PV inverter topology [Online]. Available: https://www.sma.de/fileadmin/Partner/Solaracademy/Downloads/EN/IntensivInverter-EN120910_web.pdf
- [17] G.A. Rampinelli, A. Krenzinger, F.Chenlo Romero, "Mathematical models for efficiency of inverters used in grid connected Photovoltaic systems", *Renew. Sust. Energ. Rev.*, vol. 34, pp. 578-587, Apr. 2014.
- [18] L. Davila-Gomez, A. Colmenar-Santos, M. Tawfik, M. Castro-Gil, "An accurate model for simulating energetic behavior of PV grid connected inverters", *Simulation Modelling Practice and Theory*, vol. 47, pp. 57-72, 2014.
- [19] S. Gonzalez, J. Stein, A. Fresquez, M. Ropp and D. Schutz, "Performance of utility interconnected photovoltaic inverters operating beyond typical modes of operation," *2013 IEEE 39th Photovoltaic Specialists Conference (PVSC)*, Tampa, FL, 2013, pp. 2879-2884.
- [20] S. Gonzalez, J. Neely and M. Ropp, "Effect of non-unity power factor operation in photovoltaic inverters employing grid support functions," *2014 IEEE 40th Photovoltaic Specialist Conference (PVSC)*, Denver, CO, 2014.
- [21] F. Gervasio, R. A. Mastromauro and M. Liserre, "Power losses analysis of two-levels and three-levels PWM inverters handling reactive power," *2015 IEEE International Conference on Industrial Technology (ICIT)*, Seville, 2015.
- [22] A. Anurag, Y. Yang and F. Blaabjerg, "Thermal Performance and Reliability Analysis of Single-Phase PV Inverters With Reactive Power Injection Outside Feed-In Operating Hours," *IEEE Journal of Emerging and Selected Topics in Power Electronics*, vol. 3, no. 4, pp. 870-880, Dec. 2015.
- [23] S. M. Sreechithra, P. Jirutitijaroen and A. K. Rathore, "Impacts of reactive power injections on thermal performances of PV inverters," *IECON 2013 - 39th Annual Conference of the IEEE Industrial Electronics Society*, Vienna, 2013.
- [24] ABB Datasheet, [Online]. Available: https://library.e.abb.com/public/45da04a637be47de8c1ebb696093864f/TRIO-20.0-27.6_BCD.00379_EN_RevG.pdf
- [25] N. Mohan, T. M. Undeland, W. P. Robbins, *Power Electronics: Converters Applications and Design*, New York: Wiley, 2003.
- [26] Islam Md. Rabiul, Guo Youguang, Zhu Jianguo, "Power Converters for Small- to Large-Scale Photovoltaic Power Plants" in *Power Converters for Medium Voltage Networks*, Springer-Verlag Berlin Heidelberg 2014
- [27] D. Graovac, M.Pürschel, Infineon 2009 Application Note "IGBT Power Losses Calculation Using the Data-Sheet Parameters", [Online]. Available: http://dabocorp.com/?module=file&act=procFileDownload&file_srl=894&sid=90d86d3d1f62faadc1186a680db80712
- [28] ABB Applic. Note 5SYA 2053-04 "Applying IGBTs" [Online]. Available: https://library.e.abb.com/public/ab119704d4797bc283257cd3002ac5e0/Apply%20IGBTs_5SYA%202053-04.pdf
- [29] Mohsen Shayestegana, et al "An overview on prospects of new generation single-phase transformerless inverters for grid-connected photovoltaic (PV) systems", *Renew. Sust. Energ. Rev.* vol. 82, pp. 515-530, 2018
- [30] E. Koutroulis and F. Blaabjerg, "Methodology for the optimal design of transformerless grid-connected PV inverters," *IET Power Electronics*, vol. 5, no. 8, pp. 1491-1499, Sep. 2012
- [31] EMC filter [Online]. Available: https://en.tdk.eu/inf/30/db/emc_2014/B86305L.pdf
- [32] Datasheet Database Powered by IEEE [Online]. Available: <http://www.datasheets360.com/>
- [33] IXYS IGBT [Online]. Available: [http://ixapps.ixys.com/Datasheet/DS100444A\(IXYH40N90C3\).pdf](http://ixapps.ixys.com/Datasheet/DS100444A(IXYH40N90C3).pdf)
- [34] IXYS diode [Online]. Available: <http://ixapps.ixys.com/datasheet/dsi30-12a.pdf>
- [35] Fairchild Semiconductor IGBT [Online]. Available: <http://www.onsemi.com/PowerSolutions/product.do?id=FGA30N120FTD>
- [36] B. Sahan, S. V. Araújo, C. Nöding and P. Zacharias, "Comparative Evaluation of Three-Phase Current Source Inverters for Grid Interfacing of Distributed and Renewable Energy Systems," *IEEE Trans. on Power Electronics*, vol. 26, no. 8, pp. 2304-2318, Aug. 2011.
- [37] GetData Graph Digitizer, Available [Online]: <http://getdata-graph-digitizer.com/download.php>
- [38] Dileep G, S.N. Singhb, "Selection of non-isolated DC-DC converters for solar photovoltaic system", *Renewable and Sustainable Energy Reviews*, 76 (2017) 1230-1247
- [39] Robert W. Erickson, Dragan Maksimović, *Fundamentals of Power Electronics, 2nd Edition*, Springer, 2001.
- [40] O. Al-Naseem, R. W. Erickson and P. Carlin, "Prediction of switching loss variations by averaged switch modeling," *APEC 2000. Fifteenth Annual IEEE Applied Power Electronics Conference and Exposition (Cat. No.00CH37058)*, New Orleans, LA, USA, 2000, pp. 242-248 vol.1.



Kyriaki - Nefeli D. Malamaki was born in 1986. She received her Diploma in Electrical and Computer Engineering from the Aristotle University in 2012. She is currently a Ph.D. student with the Electrical and Computer Engineering Department of the Aristotle University of Thessaloniki, Greece. Her research interests are in the fields of power quality, interface of renewable energy sources with the grid and power electronic converters.



Charis S. Demoulias (M'96, SM'11) was born in 1961. He received the Diploma and Ph.D. degrees in Electrical engineering from the Aristotle University of Thessaloniki, Thessaloniki, Greece, in 1984 and 1991, respectively. Currently, he is Associate Professor with the Electrical Machines Laboratory, Department of Electrical and Computer Engineering, Aristotle University of Thessaloniki. His research interests are in the fields of power electronics, harmonics, electric motion systems, and renewable energy sources.